Photoacoustic microscopy by scanning mirror-based synthetic aperture focusing technique

De Cai (蔡 德), Zhongfei Li (李忠飞), and Sung-Liang Chen (陈松良)*

University of Michigan-Shanghai Jiao Tong University Joint Institute, Shanghai Jiao Tong University, Shanghai 200240, China

**Corresponding author: sungliang.chen@sjtu.edu.cn*

Received May 10, 2015; accepted July 31, 2015; posted online August 31, 2015

Photoacoustic imaging with a synthetic aperture focusing technique (SAFT) is an effective method to improve the lateral resolution for out-of-focus regions in scanning microscopy systems, which commonly require a decent motorized scanning stage for a lateral scan of a transducer to obtain a cross-sectional image. In this study, we propose and test a photoacoustic imaging system with a scanning mirror-based SAFT (SM-SAFT) for simple and fast data acquisition, without the need for a physical scan of the transducer. Photoacoustic images of hair phantoms acquired by SM-SAFT are demonstrated, serving as a proof-of-concept experiment to show the feasibility and potential of the proposed approach.

OCIS codes: 110.5120, 180.5810, 110.6880.
doi: 10.3788/COL201513.101101.

Photoacoustic imaging is an emerging hybrid modality that combines the advantages of high optical contrast and low acoustic scattering. The absorption of short laser pulses by tissues induces a small temperature rise, causing thermal expansion through the thermoelastic effect and then the resulting emission of acoustic waves. Photoacoustic imaging has been investigated intensively during the past decade to obtain both structural and functional images, such as three-dimensional (3D) microvasculature, blood flow, and oxygenation[1–3]. The low acoustic scattering in soft biological tissues enables photoacoustic images with penetration depths up to several centimeters with diffraction-limited ultrasonic spatial resolution[1]. To realize high-resolution photoacoustic microscopy (PAM), high lateral resolution is achieved either by optical focusing[4,5] or by acoustic focusing using a focused transducer with a high numerical aperture (NA)[6–9]. The former and the latter are known as optical-resolution PAM and acoustic-resolution PAM (AR-PAM), respectively[10].

In the case of AR-PAM, Zhang *et al.* adopted a spherically focused transducer with a high central frequency of 50 MHz and a large NA to achieve high resolution and good signal-to-noise ratio (SNR)[6]. A lateral resolution of 45 μm at the focal zone and an axial resolution of 15 μm were achieved. Photoacoustic images of tissues such as melanoma[6] and sentinel lymph nodes[8] were successfully acquired by the system. Unfortunately, due to the high NA of the focused transducer of the system, the high lateral resolution is guaranteed only within the acoustic focus, while the lateral resolution outside the acoustic focus is deteriorated significantly. One solution to effectively improve the out-of-focus lateral resolution involves using a synthetic aperture focusing technique (SAFT), which has been applied to ultrasound[11,12] and photoacoustic imaging[13–18]. SAFT is mainly a delay-and-sum algorithm. Photoacoustic imaging with one-dimensional (1D) and two-dimensional (2D) SAFT have been explored.

Photoacoustic imaging with SAFT and coherence weighting was demonstrated to improve lateral resolution by 400%–800% and to increase the SNR by 7–23 dB using a needle hydrophone with an active size of 200 μm[13]. Later, a virtual detector-based SAFT for PAM was explored with a large NA transducer[14]. Significant improvement of the degraded lateral resolution in the out-of-focus region was demonstrated in both the phantom and *in vivo* experimental results. A 2D SAFT for PAM was also studied to improve the anisotropy of the resolution in the 1D SAFT[16]. Another fast-scanning PAM system for photoacoustic imaging with SAFT was implemented, requiring the use of two decent 1D piezoelectric scanning stages to achieve real-time scanning[18,19]. In these works, the hydrophone or the transducer was mechanically scanned with a precision translation stage. Alternatively, a multi-element SAFT photoacoustic imaging system was realized to acquire the photoacoustic signal using a 128-element linear ultrasonic transducer array to achieve fast imaging[20].

In this study, we proposed and developed a scanning mirror-based SAFT (SM-SAFT) photoacoustic imaging system using a simple and fast mirror scan that does not require a fast translation stage for the physical scan of a transducer or a multi-element transducer array for fast imaging. We investigated the feasibility of the SM-SAFT by studying the PAM images of hair phantoms.

In AR-PAM, a focused transducer is employed to provide the ultrasonic focus. The focal point of the transducer can be considered as a virtual point detector for the virtual-detector SAFT[14]. When the pulsed laser illuminates biological tissues, the generated photoacoustic waves can be detected by the virtual detector within a certain solid angle. If a linear scan is performed, the photoacoustic radiation patterns from the virtual detectors at

neighboring positions can be used for synthetic-aperture focusing. The determination of the number of neighboring positions is discussed later. By applying appropriate delays relative to the virtual point detectors at different scanning positions and then summing the delayed signals[14], the virtual-detector SAFT can be realized by

$$S_{\mathrm{SAFT}}(t) = \sum_{i=0}^{N-1} S(i, t - \Delta t_i), \tag{1}$$

where $S(i,t)$ is the detected signal at scanning position i, and Δt_i is the time delay applied to the signal from scanning position i. N is the maximum number of scanning positions included in the sum of Eq. (1) and is determined by the angular extent of the photoacoustic radiation pattern. Note that it is not necessary to use a linear scan in Eq. (1). For example, an arc scan of the virtual point detectors also works for the virtual-detector SAFT, as long as the photoacoustic detection pattern of the virtual detector at its current position overlaps with that of the virtual detector at neighboring positions.

Besides the virtual-detector SAFT, a data-dependent coherence factor (CF) can be used as a weighting factor for each SAFT imaging point to further improve the SNR and spatial resolution[14]. The quantity of the CF ranges from 0 to 1. A low CF value is due to the destructive summation of the delayed signals at the side lobes of the focused transducer, while a high CF value results from constructive summation at the main lobe. The SAFT image is multiplied by the corresponding CF map on a point-by-point basis, which suppresses the side lobes in the SAFT. After applying the SAFT and CF, the image quality in the out-of-focus region can be improved.

In the SM-SAFT, the detector is kept stationary, and the galvanometer mirror is scanned to reflect the photoacoustic radiation field during data acquisition. We illustrate the idea using a point detector placed along the x axis, as shown in Fig. 1(a). The mirror is originally placed at a certain angle θ (e.g., 45°) and is to be tilted with respect to the origin O. The photoacoustic waves are detected through the path to the mirror, which is determined as if the detector is placed at its mirrored position, and then reflected to the detector, as shown in Path 1 in Fig. 1(a). When the mirror is tilted to a certain angle at $\theta + \Delta\theta$, the photoacoustic waves propagate along another path based on the same rule as in the case of the angle at θ, which is shown in Path 2 in Fig. 1(a). The real propagating paths of the photoacoustic fields are plotted in solid lines, while the equivalent paths from the mirror to the mirrored position of the detectors are plotted in dashed lines. As an angle scan is performed to the mirror, the detector is equivalently scanned along its mirrored positions. Thus, the SAFT can be implemented by considering that the detector is scanned at its mirrored positions, usually along an arc path. Similarly, the focused transducer can also be equivalently scanned along the mirrored positions of the virtual point detector to realize the virtual-detector SM-SAFT, as illustrated in Fig. 1(b).

A SM-SAFT system was built to facilitate this study, as shown in Fig. 2. A lamp-pumped solid-state Q-switched laser (LPS-S-532, Changchun New Industries Optoelectronics Tech. Co., China) was employed to provide laser pulses at a wavelength of 532 nm, a pulse duration of 8 ns, and a pulse repetition frequency (PRF) of 20 Hz. The laser beam with a diameter of ~7 mm was used to illuminate the sample through free space. In this system, the laser worked in an external trigger mode. A focused transducer with a 10 MHz center frequency, ~80% nominal bandwidth, and an active element diameter of ~10 mm (V327-SU, Panametrics NDT, Waltham, MA) was employed to detect the photoacoustic waves. The focal length of the transducer is 15 mm. The galvanometer scanner was placed with its scanning center 11.5 mm away from the aperture center of the transducer, and was tilted at about 45° to the x axis. The sample, the mirror, and the transducer were all immersed in water, serving as acoustic coupling media, while the electrical part of the galvanometer (along the y direction) was isolated from the water. A PC-controlled analog output module (NI cRIO-9263, National Instrument) synchronized the laser triggering and the mirror scanner. The detected photoacoustic signals were first amplified by an acoustic amplifier (5077PR, Panametrics NDT) and then recorded by a data acquisition card (PCIe-9852, ADLINK Technology, Inc.) at a 200 MHz sampling rate. No signal averaging was applied during data acquisition. The acquired data were stored in a personal computer for further SAFT processing.

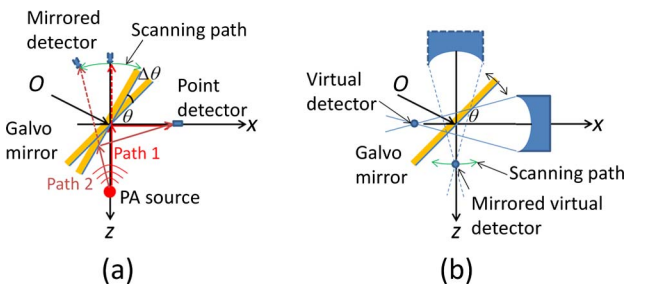

Fig. 1. Schematic illustration of the SM-SAFT. (a) Point detector. (b) Virtual detector.

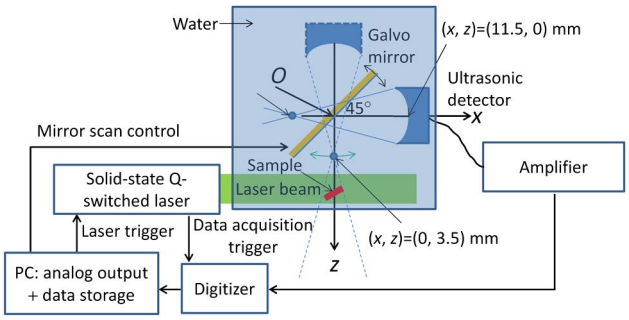

Fig. 2. Schematic of the experimental setup for the SM-SAFT.

Table 1. Lateral Width (−6 dB) and SNR Values

Target # (From Top)	Original (μm/dB)	SAFT + CF (μm/dB)
1	477/34	365/30
2	665/32	400/36
3	856/32	445/38
4	1063/30	585/41
5	1221/29	755/39
6	1345/29	855/39

The SM-SAFT system was evaluated by a cross-sectional view of a human hair-thread phantom fixed with 1% agar. The photoacoustic hair-thread phantom was placed at six different depths, separated by ∼1 mm, along the axial direction of the mirrored, focused transducer. For easy display, images at various depths were montaged into one image. The virtual detector was at the coordinate $(x, z) = (-3.5, 0)$, and the rotation center of the scanning mirror was at O (0, 0), as shown in Fig. 2. That is, the mirrored virtual detector was at the coordinate $(x, z) = (0, 3.5)$ mm, which was ∼1 mm above the uppermost hair thread. The step size of the scanning angle was ∼0.38°, and the number of scanning positions was 40 in this case. The arc scan with small curvature was then determined. The photoacoustic image of the hair phantom is shown in Fig. 3, where the original photoacoustic image, the SAFT image, and the SAFT + CF weighted image are in Figs. 3(a–c), respectively. The three images are displayed on the same linear grayscale. The vertical axis is the depth from the rotation center of the mirror, and the horizontal axis is the lateral position. In Fig. 3(a), the hair threads farther away from the mirrored virtual detector have a wider lateral extent, indicating poorer lateral resolution, which is due to the limited depth of focus of the transducer. The final SAFT + CF weighted image is presented in Fig. 3(c); it shows improved lateral resolution and reduced background noise compared with the original image shown in Fig. 3(a). After applying SAFT + CF, the −6 dB width of the imaged hair is improved from 477–1345 to 365–855 μm, depending on the distance from the virtual detector. The SNR, defined as the ratio of the maximal intensity at the hair position to the average noise intensity, is improved by up to 10 dB in Fig. 3(c) from Fig. 3(a). The −6 dB lateral width and the SNR at all the imaging depths are given in Table 1. As can be seen, the photoacoustic images by SM-SAFT demonstrate similar advantages as those taken by mechanically scanned SAFT (not performed in this work)[13–18].

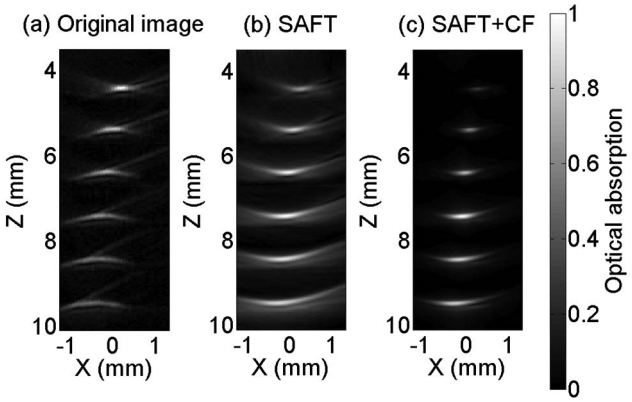

Fig. 3. Images of the hair-thread phantom scanned at various depths: (a) Original image, (b) SAFT image, and (c) SAFT + CF weighted image.

Using a laser system working at a PRF of 20 Hz, the data acquisition time for 40 scanning positions was only ∼2 s. The acquisition speed can be further enhanced by using a laser with a higher PRF. An up to 0.5 MHz PRF nanosecond laser is available and has been used for photoacoustics[21]. Additionally, by employing a high-PRF laser, more signal averaging can be applied to the SM-SAFT to improve the SNR. A weaker intensity at the near-focus position in Fig. 3(c) can be improved by applying the spatial impulse response SAFT[18]. Due to a finite aperture of the focused transducer, a limited tilt angle was used in the virtual-detector SM-SAFT to avoid the hit between the mirror and the transducer, leading to a restricted size of the synthetic aperture. We expect, however, that a larger aperture of SM-SAFT can be synthesized, thereby possibly resulting in a higher lateral resolution, by employing a small size detector (i.e., the case of Fig. 1(a)) such as a micro-ring ultrasound detector (active element size: 60 μm)[22] or a fiber-optic Fabry–Perot ultrasound detector (active element size: ∼10 μm)[23].

We also conducted a 3D photoacoustic imaging of some knotted hairs to demonstrate a method for 3D SM-SAFT. A 2D scan was performed with the fast mirror scan along the x axis and a relatively slow mechanical scan using a motorized translation stage along the y axis. To enlarge the imaging area and reduce the total scanning time, a step size of 200 μm in the mechanical scan was used. A side-view (YZ plane) photograph of the phantom consisting of five hairs is shown in Fig. 4(a). Figures 4(b) and 4(c) are the original and the SAFT + CF weighted photoacoustic images, in which the maximum amplitude projection (MAP) images along the YZ and XZ planes are plotted, where the 1D SAFT was performed along the x axis in view of the hair placed along the y axis[16,17].

The YZ MAP images in both Figs. 4(b) and 4(c) show good agreement with Fig. 4(a). Figure 4(c) shows improved SNR compared with Fig. 4(b). The SAFT + CF weighted image with improved SNR reveals a clearer identification of the hair threads than the original image. Note that the hair threads with a more oblique orientation are less visible than those with a more horizontal orientation, which is due to the limited-view problem of the transducer[24,25]. As for the XZ MAP images, the lateral extent in the x direction is improved in Fig. 4(c) compared with Fig. 4(b), because SAFT + CF weighting was performed for each B scan along the x direction.

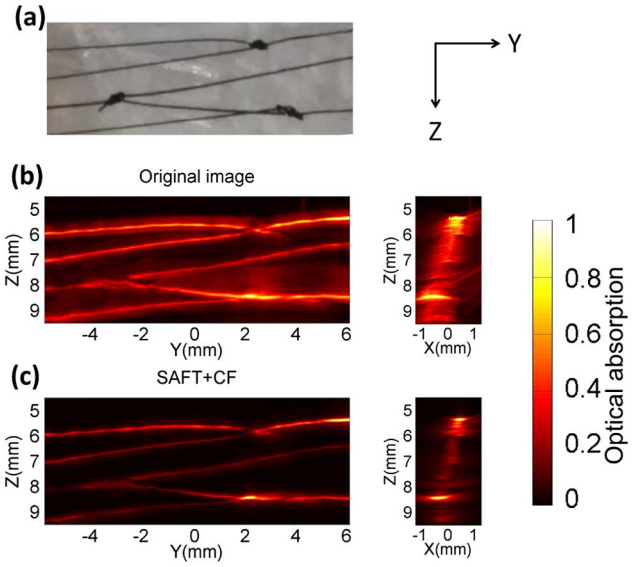

Fig. 4. 3D demonstration of the PAM images of hairs by SM-SAFT. (a) The photograph; 2D MAP images on the YZ and XZ planes, (b) Original image, and (c) SAFT + CF weighted image.

In conclusion, the SM-SAFT provides a fast scan that improves the lateral resolution in the out-of-focus region of a PAM system. The improved lateral resolution and SNR are verified by imaging the phantom of the hair thread at various depths. We also demonstrate 3D photoacoustic imaging of several knotted hairs with 2D scans: the mirror scan along the fast axis, and the mechanical scan along the slow axis. The proposed system suggests a simple and quick scan, which can be used for SAFT implementation. Employing a laser with a higher PRF to demonstrate even faster data acquisition for SM-SAFT and its application in studying the fast dynamics of photoacoustics are of great interest for future work.

This work was supported by the National Natural Science Foundation of China (No. 61405112) and the Shanghai Pujiang Program (No. 14PJ1404400).

References

1. L. V. Wang, Nat. Photon. **3**, 503 (2009).
2. V. Ntziachristos, Nat. Methods **7**, 603 (2010).
3. W. Song, Q. Wei, R. Zhang, and H. Zhang, Chin. Opt. Lett. **12**, 051704 (2014).
4. K. Maslov, H. F. Zhang, S. Hu, and L. V. Wang, Opt. Lett. **33**, 929 (2008).
5. S.-L. Chen, Z. Xie, L. J. Guo, and X. Wang, Photoacoustics **1**, 30 (2013).
6. H. F. Zhang, K. Maslov, G. Stoica, and L. V. Wang, Nat. Biotechnol. **24**, 848 (2006).
7. H. F. Zhang, K. Maslov, and L. V. Wang, Nat. Protoc. **2**, 797 (2007).
8. K. H. Song, E. W. Stein, J. A. Margenthaler, and L. V. Wang, J. Biomed. Opt. **13**, 054033 (2008).
9. R. Ma, S. Söntges, S. Shoham, V. Ntziachristos, and D. Razansky, Biomed. Opt. Express **3**, 1724 (2012).
10. Z. Wu, M. Sun, Q. Wang, T. Liu, N. Feng, J. Liu, and Y. Shen, Chin. Opt. Lett. **12**, 121701 (2014).
11. C. Frazier and W. O'Brien, IEEE Trans. Ultrason. Ferroelectr. Freq. Control **45**, 196 (1998).
12. M.-L. Li, W.-J. Guan, and P.-C. Li, IEEE Trans. Ultrason. Ferroelectr. Freq. Control **51**, 63 (2004).
13. C.-K. Liao, M.-L. Li, and P.-C. Li, Opt. Lett. **29**, 2506 (2004).
14. M.-L. Li, H. F. Zhang, K. Maslov, G. Stoica, and L. V. Wang, Opt. Lett. **31**, 474 (2006).
15. S. Park, A. B. Karpiouk, S. R. Aglyamov, and S. Y. Emelianov, Opt. Lett. **33**, 1291 (2008).
16. Z. Deng, X. Yang, H. Gong, and Q. Luo, J. Appl. Phys. **109**, 104701 (2011).
17. Z. Deng, X. Yang, H. Gong, and Q. Luo, Opt. Express **20**, 7555 (2012).
18. J. Turner, H. Estrada, M. Kneipp, and D. Razansky, Opt. Lett. **39**, 3390 (2014).
19. H. Estrada, J. Turner, M. Kneipp, and D. Razansky, Laser Phys. Lett. **11**, 045601 (2014).
20. X. Jia and S. Yang, Eur. Phys. J.-Appl. Phys. **52**, 30901 (2010).
21. D. A. Nedosekin, M. Sarimollaoglu, E. V. Shashkov, E. I. Galanzha, and V. P. Zharov, Opt. Express **18**, 8605 (2010).
22. B.-Y. Hsieh, S.-L. Chen, T. Ling, L. J. Guo, and P.-C. Li, Opt. Express **20**, 1588 (2012).
23. T. J. Allen, E. Zhang, and P. C. Beard, Proc. SPIE **9323**, 93230Z (2015).
24. J. Gateau, T. Chaigne, O. Katz, S. Gigan, and E. Bossy, Opt. Lett. **38**, 5188 (2013).
25. Y. Zhou, G. Li, L. Zhu, C. Li, L. A. Cornelius, and L. V. Wang, J. Biophoton. (2015), doi:10.1002/jbio.201400143.